

Two ridge ratio criteria for multiple change point detection in tensors

Jiaqi Huang¹, Junhui Wang², Xuehu Zhu³ and Lixing Zhu^{*1}

¹ *Beijing Normal University*

² *City University of Hong Kong*

³ *Xi'an Jiaotong University*

June 28, 2022

Abstract

This paper proposes two novel criteria for detecting change structures in tensor data. To measure the difference between any two adjacent tensors and to handle both dense and sparse model structures of the tensors, we define a signal-screening averaged Frobenius distance for the moving sums of tensor data and a signal-screening mode-based Frobenius distance for the moving sums of slices of tensor data. The latter is particularly useful when some mode is not suitable to be included in the Frobenius distance. Based on these two sequences, we construct two signal statistics using the ratios with adaptive-to-change ridge functions respectively, to enhance the detection capacity of the criteria. The estimated number of changes and their estimated locations are consistent to the corresponding true quantities in certain senses. The results hold when the size of the tensor and the number of change points diverge at certain rates, respectively. Numerical studies are conducted to examine the finite sample performances of the proposed methods. We also analyze two real data examples for illustration.

KEY WORDS: Adaptive-to-change ridge; Change structure of tensor; Ridge ratio criteria; Signal-screening averaged Frobenius distance; Signal-screening mode-based averaged Frobenius distance.

1. Introduction

One of the challenges in the age of big data is heterogeneity. The complexity of the data generation mechanism cannot be fully captured by classical statistical models aimed at studying independent and identically distributed data. Significantly when the data is collected over time, its generation mechanism may change over time, leading to possible structural changes. A commonly adopted assumption is that data structure may only change at times while remaining stationary between two adjacent change points.

This paper focuses on tensor data that frequently arise in many fields. Different definitions of structural changes have been adapted to the nature of applications. For example, Mahyari et al. (2017) aimed at identifying significant changes in network structure over all subjects. They used the Grassmann distance between the low-rank approximations of two tensors at adjacent times, and identified change points as the local maximizer of the Gassmann distance. This method assumes that the Grassmann distance follows a Gaussian distribution, and the issue of false-positive exists. Al-Sharora et al. (2017) constructed two tensors through adjacency matrices and used a Frobenius norm-based normalized cost function to identify change points. Zhan et al. (2021) performed HSI-MSI fusion to obtain high-resolution spectral and spatial images, calculated the differences between the fusion images at two different time points, and used the classification method. That is, based on the Frobenius norm, the generalized tensor regression method is used to divide the differences into several small tensors. Though empirical success has been reported, formal theoretical guarantees of the methods above are still lacking.

For dynamic network data or order-two tensors, Wang et al. (2021) and Zhao et al. (2019) respectively defined the CUSUM-based and MOSUM-based Frobenius distances and chose respective thresholds to identify local maximizers associated with locations of the change points. Both methods rely on several tuning parameters, such as the sparsity level and the thresholds. Particularly, to identify all possible local maximizers associated with the locations of the change points, the thresholds in the MOSUM-based methods proposed by Zhao et al. (2019) and Wang et al. (2021) are related to the unknown minimum magnitude of the changes. Thus, determining the threshold is an issue, and they gave two recommendations for practical use.

In this paper, the tensors are deemed changed when any element of the tensor has changed, and we propose two novel criteria to accommodate different situations. Our contributions can be summarized as follows.

First, to adapt both dense and sparse model structures, Wang et al. (2021), for the dynamic networks, introduced a notion of sparsity level. But how to estimate this level remains unknown. We, in this paper, define a signal-screening averaged Frobenius distance between two adjacent tensors in a sequence of the moving sums (MOSUM) as the measure for changes (see, Kolda and Bader (2009), Venetsanopoulos (2013) and Bi et al. (2021)). This distance is the averaged Frobenius distance over the remaining signal elements after ruling out those non-signal elements of ‘small’ values of MOSUM (see, e.g., Cho and Fryzlewicz (2015)). We write it as the SF-distance in short. The new Frobenius distance is guarded against being spuriously large, which may cause overestimation when the number of elements is large (see, e.g., Cho and Fryzlewicz (2015)), or spuriously small, which may cause underestimation if the average over its number of elements is considered. As a generic methodology, our

method is robust against distributions. It can also be applied to tensors of order-one (vector), order-two (matrix), and higher-order.

Second, most existing MOSUM-based or CUSUM-based methods heavily rely on the fact that the changes arrive at the maxima, and their estimation consistency can be derived when the threshold is properly chosen. This is an issue as the magnitudes of the changes are usually unknown. We define a sequence of ratios between any two adjacent SF-distances with an adaptive-to-change ridge function to circumvent this difficulty. We will see an informative periodogram of this newly proposed signal statistic with the minima of zero arrived at $z_k - 2\alpha_n + 1$ and the maxima of infinity arrived at $z_k - \alpha_n$. Here z_k 's are the locations of the changes, and α_n is the window size of the moving sums. Thus, the thresholding values (in theory, any value between 0 and 1 when we search for the minima) can be easily chosen. The computation can be fast as the detection for all change points is simultaneously implemented. Plot of the signal statistic can also assist the detection. The estimation consistency for the locations and the number of change points can be derived.

Third, using the adaptive-to-change ridge function can enhance the detection capacity of the criteria than using a constant ridge as in Zhao et al. (2021) for detecting univariate mean changes. The original purpose of using diminishing ridge is to make the undefined $0/0$ ratio be 1 such that the detection becomes easy. The adaptive-to-signal ridge function goes to infinity in the segments without involving change points. Thus, the values of the signal statistic can tend to one at a much faster rate than that with a constant ridge so that the curve oscillation at the sample level can be alleviated and false changes could be reduced.

Fourth, some mode of the tensor may have special meaning, such as subjects, such that the Frobenius norm for all elements may not be suitable, see, e.g., Mahyari et al. (2017). Also, when a mode has a larger size than the others (see, e.g., Zhang et al. (2018)), excluding this mode from the Frobenius distance is helpful to alleviate the dimensionality problem. To accommodate such situations, we propose a mode-based signal-screening Frobenius distance, where the signal-screening averaged Frobenius distance is defined on all other modes. Thus, the distance is a vector, and the ridge ratios form a vector sequence. We then define a signal statistic that is the minimum of all the elements of the vector.

Fifth, the asymptotic studies on the signal statistics are of theoretical interest. Although the statistics are empirical versions of their corresponding functions at the population level, the inconsistency in some non-negligible segments occurs. Thus, we will give detailed analysis to identify these segments and study the asymptotic behaviors of the signal statistics in these segments. We will also propose an algorithm to prevent the proposed method from falling into these segments so that the estimated number and locations of changes are still consistent. Furthermore, the consistency is established under much milder conditions; for instance, the required spacing between any two adjacent change points is shorter than in Zhao et al. (2021).

The remainder of the paper is organized as follows. Section 2 introduces the problem and notion of change point detection in tensors and suggests two criteria to detect change points. Section 3 presents the consistency of the estimated number of changes and the estimated locations in a certain sense. Section 4 includes simulation studies, including the cases with tensors of order-one, order-two, and higher-order. We find that our method can have better performance in the detection when the

number of tensor elements gets larger. This dimensionality blessing phenomenon, particularly in dense cases, might suggest that the new methods might not be seriously affected by the dimensionality. Section 5 includes the illustrative analyses for two real data examples. Section 6 discusses the merits and limitations of the new methods, particularly the choice of tuning parameters. All the technical proofs are included in the Supplementary Materials.

2. Methodology Development

2.1 Preliminary

Let $\mathcal{X}_i \in \mathbb{R}^{p_1 \times \dots \times p_\kappa}$, $i = 1, 2, \dots, n$ be independent order- κ tensors satisfying the model as follows

$$\mathcal{X}_i = E(\mathcal{X}_i) + \mathcal{E}_i, i = 1, 2, \dots, n, \quad (2.1)$$

where \mathcal{E}_i 's are independent error terms with zero mean. Here, the order κ is the number of dimensions, and each dimension is called a mode. The element $(i_1, i_2, \dots, i_\kappa)$ of tensor \mathcal{X}_i is denoted by $\mathcal{X}_{i, i_1 i_2 \dots i_\kappa}$. If we fix the mode- l index of the tensor to be i_l , then the other $(\kappa - 1)$ -dimensional sections of a tensor are called the i_l -th mode- l slice. Thus, a κ th-order tensor is a κ -dimensional array with κ modes (see more details in Kolda and Bader (2009), Venetsanopoulos (2013) and Bi et al. (2021)).

Assume that there are K change points; that is $1 = z_0 < z_1 < \dots < z_k < \dots < z_K <$

$z_{K+1} = n$, which divide the original sequence to $K + 1$ segments so that

$$E(\mathcal{X}_i) = \mathcal{M}^{(k)}, i = z_{k-1} + 1, \dots, z_k.$$

Write $\alpha_n^* = \min_{1 \leq k \leq K+1} |z_k - z_{k-1}|$ as the minimum distance between any two change points. From (2.1), we can see that the classical change point detection for means (order-one tensor) and covariance matrices (order-two tensor) could be regarded as special cases.

2.2 SF distance and a signal statistic

To construct a signal statistic, we have the following steps.

The moving sums(MOSUM). Define the MOSUM of the tensor sequence as follows:

$$\mathcal{D}(i) = \frac{1}{\alpha_n} \left(\sum_{j=i}^{i+\alpha_n-1} E(\mathcal{X}_j) - \sum_{j=i+\alpha_n}^{i+2\alpha_n-1} E(\mathcal{X}_j) \right). \quad (2.2)$$

As commented before, we define the following signal-screening metric with a threshold $l_n(s) \rightarrow 0$ as $n \rightarrow \infty$:

$$\|\mathcal{A}\|_s^2 = \frac{\sum_{i_1=1}^{p_1} \sum_{i_2=2}^{p_2} \cdots \sum_{i_\kappa=1}^{p_\kappa} a_{i_1 i_2 \dots i_\kappa}^2 I(a_{i_1 i_2 \dots i_\kappa}^2 > l_n(s))}{\sum_{i_1=1}^{p_1} \sum_{i_2=2}^{p_2} \cdots \sum_{i_\kappa=1}^{p_\kappa} I(a_{i_1 i_2 \dots i_\kappa}^2 > l_n(s)) + 1/n}, \quad (2.3)$$

where $a_{i_1 i_2 \dots i_\kappa}$ denotes $(i_1, i_2, \dots, i_\kappa)$ element of the κ -order tensor \mathcal{A} and the value $1/n$ in the denominator is to avoid the undefined $0/0$ ratio. When $l_n(s) = 0$, write $\|\mathcal{A}\|_s^2$ as $\|\mathcal{A}\|_{0s}^2$.

Call $\|\mathcal{D}(i)\|_{0s}^2$ as the SF-distance. Some elementary calculations yield the following

properties of $\|\mathcal{D}(i)\|_{0s}^2$: for each $1 \leq k \leq K$

$$\|\mathcal{D}(i)\|_{0s}^2 = \begin{cases} 0 & z_{k-1} \leq i < z_k - 2\alpha_n \\ \frac{\sum_{l=1}^{\kappa} \sum_{i_l=1}^{p_l} \mathcal{D}_{i_1 i_2 \dots i_{\kappa}}^2(i)}{\sum_{l=1}^{\kappa} \sum_{i_l=1}^{p_l} I(\mathcal{D}_{i_1 i_2 \dots i_{\kappa}}^2(i) > 0) + 1/n} \nearrow & z_k - 2\alpha_n \leq i < z_k - \alpha_n \\ \|\mathcal{M}^{(k+1)} - \mathcal{M}^{(k)}\|_{0s}^2 & i = z_k - \alpha_n \\ \frac{\sum_{l=1}^{\kappa} \sum_{i_l=1}^{p_l} \mathcal{D}_{i_1 i_2 \dots i_{\kappa}}^2(i)}{\sum_{l=1}^{\kappa} \sum_{i_l=1}^{p_l} I(\mathcal{D}_{i_1 i_2 \dots i_{\kappa}}^2(i) > 0) + 1/n} \searrow & z_k - \alpha_n < i < z_k, \end{cases}$$

where \searrow and \nearrow stand for strictly increasing and decreasing, respectively.

Ridge-ratio function. According to the properties of $\|\mathcal{D}(i)\|_{0s}^2$ and $\|\mathcal{D}(i + \alpha_n)\|_{0s}^2$, we define the ridge ratio statistic at the population level as follows:

$$T(i) = \frac{\|\mathcal{D}(i)\|_{0s}^2 + c_n^*(i)}{\|\mathcal{D}(i + \alpha_n)\|_{0s}^2 + c_n^*(i)}, \quad (2.4)$$

where the ridge function $c_n^*(i)$ to be selected later is to avoid the undefined $0/0$ of $T(i)$ such that $T(i)$ is close to 1 in the segments where the moving sums in both $\|\mathcal{D}(i)\|_{0s}^2$ and $\|\mathcal{D}(i + \alpha_n)\|_{0s}^2$ involve no locations of change points. When we use an adaptive-to-change ridge function $c_n^*(\cdot)$, Figure 1 presents the curves of $\|\mathcal{D}(\cdot)\|_{0s}^2$ and $T(\cdot)$ for a toy example, showing two very interesting patterns. From the curve of $\|\mathcal{D}(\cdot)\|_{0s}^2$, we can see that each spike uniquely corresponds to a change point. As discussed in Zhao et al. (2019) although $\|\mathcal{D}(\cdot)\|_{0s}^2$ can indicate the locations and number of changes, the unknown magnitudes of the maxima of $\|\mathcal{D}(\cdot)\|_{0s}^2$ brings up the issue of determining a proper threshold. In contrast, the curve of $T(\cdot)$ with local minima of zero and local maxima of infinity can greatly help determine the threshold. Further, different curve patterns of $T(i)$ may occur when the spacings between two adjacent change points are larger than $3\alpha_n$, $2\alpha_n + f$ or $2\alpha_n$, where $f \in (0, \alpha_n)$. Figure 1 gives the basic

idea. More details will be presented in the next section, and the detailed calculation can be found in the supplementary material. Briefly speaking, when the spacing is longer than $3\alpha_n$, $T(i)$ monotonically decreases on the left-hand side of $z_k - 2\alpha_n + 1$, drops to 0 at $z_k - 2\alpha_n + 1$, and increases up to infinity. In the last two scenarios, $T(i)$ monotonically decreases to a local minimum first and then suddenly jumps up to one in the interval with length $f + 1$, $0 \leq f < \alpha_n$, and immediately drops down to another local minimum and follows an up to infinity. All the local minimizers $z'_k - 2\alpha_n + 1$ at the right-hand sides of the discontinuous locations in all such intervals correspond to the change points. As the local minima are zero, the threshold for change point detection can be easily determined.

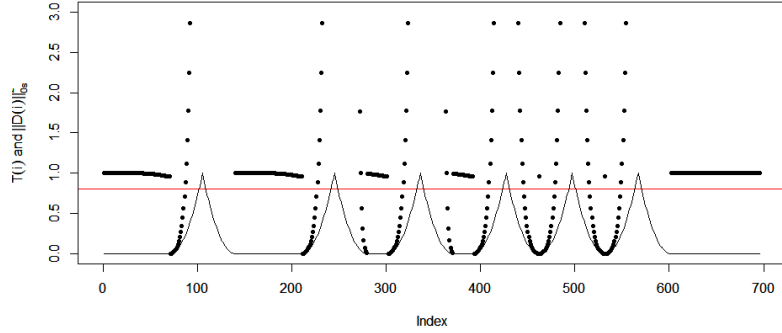


Figure 1. The solid line is for $\|\mathcal{D}(i)\|_{0_s}^2$ and the dotted line for $T(i)$.

The adaptive-to-change ridge function. Here, we give the formula of the ridge function, for a $\nu > 1/2$ and any constant s_1 ,

$$c_n^*(i) = \frac{s_1 \epsilon_n (\log n)^\nu}{I(i \in \mathcal{S}^*) + \frac{1}{n}} \quad (2.5)$$

where $\mathcal{S}^* = \{i : \sum_{l=1}^{\kappa} \sum_{i_l=1}^{p_l} I([\mathcal{D}_{i_1 i_2 \dots i_\kappa}(i)]^2 > 0) > 0\}$ and $\epsilon_n = \frac{(\log n)^{\frac{1}{2} + \epsilon}}{\sqrt{\alpha_n}}$ that is the

uniform rate of $|\mathcal{D}_{n,i_1,\dots,i_\kappa}(i) - \mathcal{D}_{i_1,\dots,i_\kappa}(i)|$ over all $\{i_1, \dots, i_\kappa\}$. The results will be presented in Section 3. First, in the segments involving no locations of changes, the denominator is very small ($1/n$ at the population level); in other words, the ridge tends to infinity such that $T(i)$ tends to one at a fast rate. Second, in the segments involving the locations of changes, $c_n^*(i)$ goes to zero with the numerator going to zero and the denominator being larger than 1. Further, $\mathcal{D}(i + \alpha_n)$ around the location $z_k - 2\alpha_n$ can be large and $\mathcal{D}(i)$ around $z_k - 2\alpha_n$ can still be small. These lead to small $T(i)$'s around $z_k - 2\alpha_n + 1$ such that we can efficiently identify the locations of the changes. We can also use large $T(i)$'s around $z_k - \alpha_n$ to identify the locations of the change points. But this is similar to using small $1/T(i)$'s. Thus, in this paper, we do not discuss its use.

From Figure 1, we can see that K change points correspond to K disjoint intervals. Thus, we can determine K disjoint intervals by using a thresholding value for $T(\cdot)$. Let $(\tilde{m}_k(\tau), \tilde{M}_k(\tau))$ denote the intervals where $\tilde{m}_k(\tau)$ and $\tilde{M}_k(\tau)$ satisfy the following conditions: for a thresholding value $\tau \in (0, 1)$,

$$T(\tilde{M}_k(\tau)) < \tau \text{ and } T(\tilde{M}_k(\tau) + 1) \geq \tau,$$

$$\text{and } \tilde{m}_k(\tau) = \tilde{M}_k(\tau) - \frac{2\sqrt{\tau}}{\sqrt{\tau}+1}\alpha_n.$$

Use the sample versions of $\mathcal{D}(i)$ and $T(i)$ to define the corresponding signal statistic. Let

$$\mathcal{D}_n(i) = \frac{1}{\alpha_n} \left(\sum_{j=i}^{i+\alpha_n-1} \mathcal{X}_j - \sum_{j=i+\alpha_n}^{i+2\alpha_n-1} \mathcal{X}_j \right)$$

and the SFD-based signal statistic is defined as

$$T_n(i) = \frac{\|\mathcal{D}_n(i)\|_s^2 + c_n(i)}{\|\mathcal{D}_n(i + \alpha_n)\|_s^2 + c_n(i)},$$

where $c_n(i)$ is an estimator of $c_n^*(i)$: for a $\nu > 1/2$ and any constant s_1 ,

$$c_n(i) = \frac{s_1 \epsilon_n (\log n)^\nu}{I(i \in \mathcal{S}) + \frac{1}{n}}, \quad (2.6)$$

and $\mathcal{S} = \{i : \sum_{l=1}^{\kappa} \sum_{i_l=1}^{p_l} I(\mathcal{D}_{n,i_1 i_2 \dots i_\kappa}^2(i) > l_n(s)) > 0\}$ is a replacement of \mathcal{S}^* in $c_n^*(\cdot)$ where $l_n(s) = s \epsilon_n (\log n)^{1/2}$, and s and s_1 are two tuning parameters. Specifically, the thresholding value 0 in $c_n^*(i)$ is replaced by $l_n(s)$ such that the set \mathcal{S}^* is replaced by \mathcal{S} and $\mathcal{D}(i)$ by $\mathcal{D}_n(i)$. Note that the results in Section 3 hold for any $\nu > 1/2$, but we recommend $\nu = 0.55$, which yields satisfactory performance in all the numerical experiments in Section 4.

Interestingly, as showed in the Supplementary Material, $\|\mathcal{D}_n(i)\|_s^2$, and $c_n(i)$ cannot respectively converge to $\|\mathcal{D}(i)\|_{0s}^2$ and $c_n^*(i)$ uniformly over all i , which further implies that the sample version $T_n(i)$ cannot converge to $T(i)$ uniformly over all i . Because of the different curve pattern of $T_n(\cdot)$ from that of $T(\cdot)$, we require a more careful choice for the intervals $(m_k(\tau), M_k(\tau))$ each containing only one local minimizer converging to that of $T(\cdot)$ in a certain sense. The inconsistency occurs in the intervals where $\|\mathcal{D}(i)\|_{0s}^2$ and $\|\mathcal{D}(i + \alpha_n)\|_{0s}^2$ take small positive values. To help understand this intuitively, we give a toy example in Figure 2 below. Theorem 1.1 in the Supplementary Materials further elaborates when the consistency of $T_n(\cdot)$ holds and when it does not, as well as how $T_n(\cdot)$ behaves when the consistency does not hold.

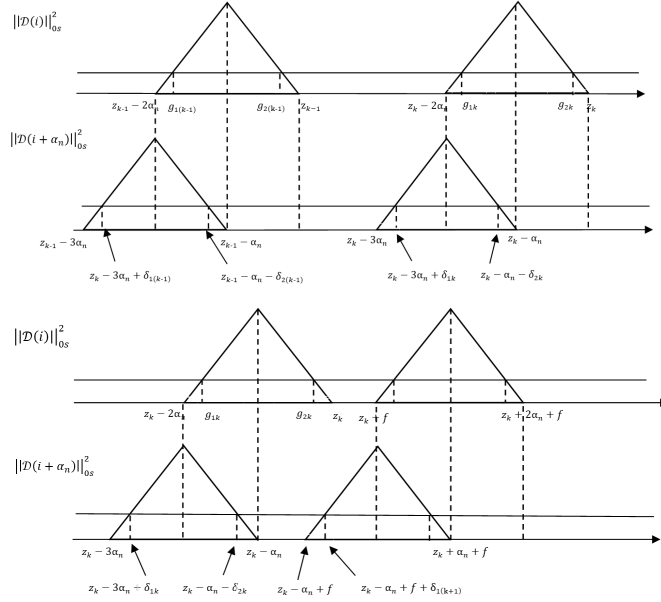


Figure 2. The upper plot is for the case where the distance between two true change points is not less than $3\alpha_n$, and the lower plot is about the case where the distance between two true change points is equal to $2\alpha_n + f$, $f \in [0, \alpha_n)$.

Choosing the intervals. Motivated by Theorem 1.1 in the Supplementary Material, we can, at the sample level, determine the disjoint intervals $(m_k(\tau), M_k(\tau))$ for $k = 1, \dots, \hat{K}$ that are the estimated intervals of $(\tilde{m}_k(\tau), \tilde{M}_k(\tau))$'s as follows. First, for a pre-determined threshold $0 < \tau < 1$, define $M_k(\tau)$ by

$$T_n(M_k(\tau)) < \tau, \quad T_n(M_k(\tau) + 1) \geq \tau \quad (2.7)$$

and let $m_k(\tau) = M_k(\tau) - \frac{2\sqrt{\tau}}{\sqrt{\tau}+1}\alpha_n$. In this paper we recommend $\tau = 0.8$. As stated in Theorem 1.1, there might be some $M_l(\tau)$'s that correspond to false change points due to the inconsistency of $T_n(\cdot)$ in some sets in which we cannot determine the behavior of $T_n(\cdot)$. We call them the uncertain sets. Then we rule out those spurious $M_l(\tau)$'s

when two conditions satisfy: $M_{l+1}(\tau) - M_l(\tau) \leq 3\alpha_n/2$, and $T_n(M_l(\tau) - \alpha_n/2) \geq 1$, where $l \in \{l : T_n(M_l) \leq \tau \text{ and } T_n(M_l + 1) > \tau\}$. This is because Theorem 1.1 offers two facts: 1). any $M_1(\tau)$ corresponding to a false change point has the distance to its nearest $M_{l+1}(\tau)$ corresponding to a true change point should be smaller than $(3 - c)\alpha_n/2$, and the distance to $M_{l-1}(\tau)$ should be longer than $(3 + c)\alpha_n/2$ for a small $c > 0$; 2). $T_n(M_1(\tau) - \alpha_n/2) \rightarrow \infty$.

Identifying the locations of change points. We can then search for local minimizers in the intervals $(m_k(\tau), M_k(\tau))$'s with the remaining $M_k(\tau)$'s, and use the minimizers plus $2\alpha_n - 1$ as the estimators \hat{z}_k 's of z_k 's. From Figure 1, we can see when the length f is not big (shorter than $\alpha_n/2$ in theory), there might exist two or more local minima in one interval(at the population level, there would be exactly two local minima). The distance between one of them plus $2\alpha_n - 1$ and z_k might not be $o(\alpha_n)$. In other words, if this local minimizer is selected, the estimation consistency is destroyed. To avoid this problem we set, for $1 \leq k \leq \hat{K}$, $r_k := \max\{\arg \min_{i \in (m_k(\tau), M_k(\tau))} T_n(i)\}$ and the estimated location is defined as $\hat{z}_k = r_k + 2\alpha_n - 1$.

2.3 The mode-based SF distance and a signal statistic

In some applications, there is a mode of the tensor having a special meaning, as commented in Mahyari et al. (2017) or a larger size than the other modes have (see, e.g., Zhang et al. (2018)). Thus, leaving this mode out from the Frobenius distance could be suitable. To deal with this situation better, we propose a notion of mode-based SF distance of MOSUM. Without loss of generality, we fix the last mode of the

tensor. Define, for $1 \leq l \leq p_\kappa$,

$$\mathcal{D}_l(i) = \frac{1}{\alpha_n} \left(\sum_{j=i}^{i+\alpha_n-1} E(\mathcal{X}_{j,l}) - \sum_{j=i+\alpha_n}^{i+2\alpha_n-1} E(\mathcal{X}_{j,l}) \right),$$

where for $1 \leq l \leq p_\kappa$, $\mathcal{X}_{j,l} \in R^{p_1 \times p_2 \times \dots \times p_{\kappa-1}}$ are the l -th slices of the tensor after fixing the κ -th mode. The corresponding sample versions of $\mathcal{D}_l(i)$ and $T_l(i)$ are

$$\mathcal{D}_{nl}(i) = \frac{1}{\alpha_n} \left(\sum_{j=i}^{i+\alpha_n-1} \mathcal{X}_{j,l} - \sum_{j=i+\alpha_n}^{i+2\alpha_n-1} \mathcal{X}_{j,l} \right),$$

and

$$T_{nl}(i) = \frac{\|\mathcal{D}_{nl}(i)\|_s^2 + c_{nl}(i)}{\|\mathcal{D}_{nl}(i + \alpha_n)\|_s^2 + c_{nl}(i)}.$$

The final MSFD-based signal statistic is defined as $T_n^v(i) = \min_{1 \leq l \leq p_\kappa} T_{nl}(i)$. For each l , the definition of $c_{nl}(i)$ is similar to $c_n(i)$ in (2.6) with \mathcal{S} being replaced by, for each $1 \leq l \leq p_\kappa$,

$$\tilde{\mathcal{S}}_l = \left\{ i : \sum_{t=1}^{\kappa-1} \sum_{i_t=1}^{p_t} I(\mathcal{D}_{nl, i_1 i_2 \dots i_{\kappa-1}}^2(i) > l_n(s)) > 0 \right\}.$$

Theorem 3.2 in Section 3 offers the estimation consistency of the locations and number of the change points. Write $T^v(\cdot)$ and $\|\mathcal{D}_l(\cdot)\|_{0_s}^2$ as the corresponding functions at the population level. To see the difference from $T(\cdot)$, two different curves of $T^v(i)$ in Figure 3 present two different scenarios. If the change points occur in all slices, $T^v(\cdot)$ have the same properties as $T(\cdot)$, see the top plot; otherwise, $T^v(\cdot)$ has a curve different from $T(\cdot)$, see the bottom plot.

Similarly, to those with $T_n(\cdot)$, we also choose the relevant intervals to identify the locations of the local minima. As $T_n^v(\cdot)$ has different asymptotic behaviors, we need some modifications, although the basic ideas are similar to that with $T(\cdot)$.

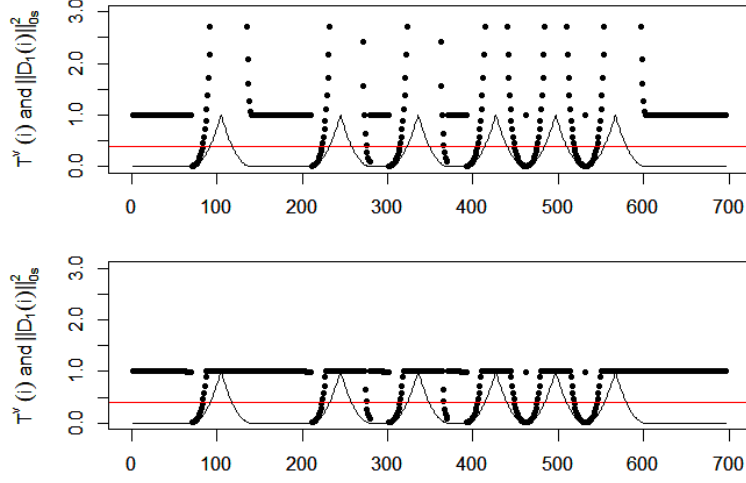


Figure 3. the curves of $\|\mathcal{D}_1(\cdot)\|_{0_s}^2$ and $T^v(\cdot)$. The dashed line is for $\|\mathcal{D}_1(\cdot)\|_{0_s}^2$ and the dot line for $T^v(\cdot)$. The upper plot presents the curve when all elements of the vector have changes at the same locations; the lower plot is for the curves when there is at least an element of the vector having changes at different locations.

Choosing the intervals. By the results of Theorem 1.2 in the Supplementary material, we similarly determine the disjoint intervals $(m_k^v(\tau), M_k^v(\tau))$ for $k = 1, \dots, \hat{K}$ as follows. First, for a pre-determined threshold $0 < \tau < 1$, define $M_k^v(\tau)$ by

$$T_n^v(M_k^v(\tau)) < \tau, \quad T_n^v(M_k^v(\tau) + 1) \geq \tau \quad (2.8)$$

and let $m_k^v(\tau) = M_k^v(\tau) - \frac{2\sqrt{\tau}}{\sqrt{\tau+1}}\alpha_n$. As $T_n^v(\cdot)$ is the minimum of $T_{nl}(\cdot)$, the values tend to be small at the sample level. We then in this paper recommend $\tau = 0.4$. As stated in Theorem 1.2, the inconsistency of $T_n^v(\cdot)$ occurs in the uncertain sets in which we cannot determine what behavior of $T_n^v(\cdot)$ is. Then, there might also exist some M_g 's that correspond to false change points. We rule out those M_g 's when $M_{g+1}(\tau) - M_g(\tau) \leq 3\alpha_n/2$, where $g \in \{g : T_n^v(M_g) < \tau \text{ and } T_n^v(M_g + 1) \geq \tau\}$. This is a different algorithm from that with $T_n(\cdot)$. It is because Theorem 1.2 offers the fact: any $M_g(\tau)$ corresponding to a possible false change point has the distance to

its nearest $M_{g+1}(\tau)$ corresponding to a true change point should be smaller than $(3 - c)\alpha_n/2$, and the distance to $M_{g-1}(\tau)$ should be longer than $(3 + c)\alpha_n/2$ for a small $c > 0$. But we no longer have the property that $T_n^v(M_g(\tau) - \alpha_n/2) \rightarrow \infty$. See it intuitively from Figure 3.

Identifying the locations of change points. This step can be similar to that with $T_n(\cdot)$ by identifying the local minimizer $r_k := \max\{\arg \min_{i \in (m_k^v(\tau), M_k^v(\tau))} T_n^v(i)\}$ for $1 \leq k \leq \hat{K}$ and the estimated location is defined as $\hat{z}_k = r_k + 2\alpha_n - 1$.

3. The asymptotic properties

This section gives the asymptotic properties of the proposed signal statistics, the estimated locations \hat{z}_k , and the estimated number \hat{K} of change points.

Firstly, we introduce some notations to be used in the following theorems. Denote $\text{Var}(\text{vec}(\mathcal{E})) =: \mathbf{\Sigma} = (\sigma_{j_1 j_2}), 1 \leq j_1, j_2 \leq p$ and $p = \prod_{l=1}^{\kappa} p_l$, where $\text{vec}(\cdot)$ represents the vectorization of a tensor. Let $\boldsymbol{\eta} = \mathbf{\Sigma}^{-\frac{1}{2}} \text{vec}(\mathcal{E})$, $a_n = \frac{(\log n)^{1+2\epsilon}}{(\log n)^{\rho_1} \alpha_n (\log np)}$, and $b_n = \frac{(a_n \alpha_n - 2C')^2}{(\log n)^{\rho_2} \log[(K+1)pn](K+1)^2}$ for three positive constants ϵ, ρ_1 and ρ_2 .

Proposition 3.1. *Assume that $\mathcal{X}_i - E(\mathcal{X}_i)$ are independent random tensors.*

(1) *Under Condition 1, when $\frac{n^2 p}{\alpha_n^4 b_n^2} \rightarrow 0$, we have the following result:*

$$\max_i \max_{i_1, i_2, \dots, i_{\kappa}} |\mathcal{D}_{n, i_1 i_2 \dots i_{\kappa}}(i) - \mathcal{D}_{i_1 i_2 \dots i_{\kappa}}(i)| = O_p \left(\frac{(\log n)^{\frac{1}{2} + \epsilon}}{\sqrt{\alpha_n}} \right). \quad (3.1)$$

(2) *Further, assume that the elements η_{ij} of $\boldsymbol{\eta}_i$ for $i = 1, 2, \dots, n; j = 1, 2, \dots, p$ are independent and identically distributed. Suppose that Conditions 2 and 3*

hold and $\frac{\alpha_n^5 \log(np)}{n^4} = o(1)$. If

$$[E|\eta_{11}|^q]^{1/q} < \infty \text{ and } \frac{(\log(np))^{3q/2} np}{\alpha_n^{q/2}} = o(1)$$

hold for some $q \geq 4$, or

$$E(\exp^{a_0 \eta_{11}}) < \infty \text{ and } \frac{(\log(np))^{\max\{7, 2(1+\beta)/\beta\}}}{\alpha_n} = o(1)$$

for some $a_0 > 0$ hold, then we have

$$\max_i \max_{i_1, i_2, \dots, i_\kappa} |\mathcal{D}_{n, i_1 i_2 \dots i_\kappa}(i) - \mathcal{D}_{i_1 i_2 \dots i_\kappa}(i)| = O_p \left(\frac{(\log(np))^{1/2+\epsilon}}{\sqrt{\alpha_n}} \right). \quad (3.2)$$

For simplicity of notation, denote $\epsilon_n = \frac{(\log n)^{\frac{1}{2}+\epsilon}}{\sqrt{\alpha_n}}$ in Part (1) and $\epsilon_n = \frac{(\log(np))^{1/2+\epsilon}}{\sqrt{\alpha_n}}$ in Part (2).

Remark 3.1. (*Allowed dimension*) This proposition shows the critical differences between Parts (1) and (2). Particularly, under additional conditions on η_{ij} , such as the IID condition as well as other conditions on its moment and tail probability (see, e.g., Theorem 1 in Chen et al. (2021)), we can see from Part (2) that the divergence rate of p can be fast while when these conditions are relaxed as in Part (1), we still have the estimation consistency of $\mathcal{D}(i)$ with a slower divergence rate of p .

In Part (1), the formulas of a_n and b_n give that

$$\frac{n^2 p}{\alpha_n^4 b_n^2} = \frac{n^2 p (\log n)^{4\rho_1 + 2\rho_2} [\log(np)]^4 \{\log[(K+1)np]\}^2 (K+1)^4}{\alpha_n^4 [(\log n)^{1+2\epsilon} - 2C'(\log n)^{\rho_1} \log(np)]^4} \rightarrow 0.$$

Take $\epsilon = \frac{\rho_1}{2} + \frac{\rho_2}{4} + 1$, then $\frac{n^2 p \{\log[(K+1)n]\}^2 [\log(np)]^4 (K+1)^4}{\alpha_n^4 [\log n]^6} \rightarrow 0$. When the number of

change points is fixed and $\alpha_n = n^{\frac{1}{2}+\nu}$ with $\nu \in (0, \frac{1}{2})$, we can see that p can be close to the order $n^{4\nu}$ and can be close to n^2 at most.

In Part (2), under the finite moment conditions, p can be at a polynomial order of n , depending on q . The larger q allows the larger dimension p . Under the exponential tail condition, p can be exponential in n .

Define $\mathcal{G} = \{i : \exists i_1, i_2, \dots, i_\kappa, \mathcal{D}_{i_1 i_2 \dots i_\kappa}^2(i) > 0 \text{ and } \mathcal{D}_{n, i_1 i_2 \dots i_\kappa}^2(i) \leq l_n(s)\}$, and $(\mathcal{G} + \alpha_n) = \{i : i - \alpha_n \in \mathcal{G}\}$. Let $g_{1k} = \arg \min_{j \in \mathcal{G}, j+1 \notin \mathcal{G}} |j - (z_k - 2\alpha_n)|$ and $g_{2k} = \arg \min_{j \in \mathcal{G}, j-1 \notin \mathcal{G}} |j - z_k|$ for $k = 1, 2, \dots, K$.

Proposition 3.2. *Under the conditions in Proposition 3.1, we have*

$$(1) \max_{i \in \mathcal{G}^c} \left| \|\mathcal{D}_n(i)\|_s^2 - \|\mathcal{D}(i)\|_{0s}^2 \right| = O_p(\epsilon_n).$$

$$(2) \text{ Let } \delta_{1k} = g_{1k} - (z_k - 2\alpha_n) \text{ and } \delta_{2k} = z_k - g_{2k}. \text{ If Condition 6 holds, then } \max_{1 \leq k \leq K} \delta_{1k} = o_p(\alpha_n) \text{ and } \max_{1 \leq k \leq K} \delta_{2k} = o_p(\alpha_n).$$

$$(3) \text{ Let } \mathcal{M}_n = \{i : T_n(i) \leq M_n(i)\}, \text{ where } M_n = o\left(\frac{c_n(i)}{\epsilon_n}\right). \text{ If Condition 2 holds, } \max_{i \in \mathcal{G}^c \cap (\mathcal{G} + \alpha_n)^c \cap \mathcal{M}_n} |T_n(i) - T(i)| = o_p(1).$$

The above results are the basis for obtaining the consistency of the estimated locations and number of change points when the signal statistic $T_n(\cdot)$ is used. There may exist some intervals with length $o(\alpha_n)$ such that $\|\mathcal{D}_n(i)\|_s^2$ does not converge to $\|\mathcal{D}(i)\|_{0s}^2$, and similarly for $T_n(\cdot)$. Part (3) is a part of the results in Theorem 1.1 in the Supplementary material. We will, in this theorem, give some detailed analysis of the inconsistency and some more asymptotic behaviors of $T_n(\cdot)$ in the set $\mathcal{G} \cup (\mathcal{G} + \alpha_n)$. Importantly, we will show that this set is sufficiently small and does not influence the

choice of $M_k(\tau)$ and the consistency of \hat{z}_k . The following theorem states the results.

Define $\hat{z}_k = 0$ if $\hat{K} < k \leq K$.

Theorem 3.1. *Under the conditions in Proposition 3.2, when Conditions 6 and 7 hold, $\alpha_n^* \geq 2\alpha_n$ and $\frac{n}{K\alpha_n^*} \rightarrow \infty$, we have*

$$Pr(\hat{K} = K) \rightarrow 1,$$

and the estimators $\{\hat{z}_1, \hat{z}_2, \dots, \hat{z}_{\hat{K}}\}$ have

$$Pr \left\{ \max_{1 \leq k \leq K} \left| \frac{\hat{z}_k - z_k}{\alpha_n} \right| < \epsilon \right\} \rightarrow 1$$

for every $\epsilon > 0$.

Because of the similar construction of all elements $T_{nl}(\cdot)$ of $T_n^v(\cdot)$, the consistency and inconsistency in different sets can be similarly investigated as the above for $T_n(\cdot)$. The estimation consistency of the locations and number of change points can still retain. We then do not give the results about $T_{nl}(\cdot)$ while directly stating the asymptotic results about the estimated locations and number of change points when the signal statistic $T_n^v(\cdot)$ is used.

Theorem 3.2. *Under the conditions in Proposition 3.2, when Conditions 6 and 7 hold, $2\alpha_n \leq \alpha_n^*$, and $\frac{n}{K\alpha_n^*} \rightarrow \infty$, the results in Theorem 3.1 hold true with respect to $T_n^v(\cdot)$.*

4. Simulations

To examine the performances of the proposed criteria, we conduct the simulations

with several different model settings and compare our methods with existing competing methods, if any. For order-one tensor (vector), we compare with the E-Divisive method (Matteson and James (2014)), the change point detection through the Kolmogorov-Smirnov statistic (Zhang et al. (2017)), the change point detection via sparse binary segmentation (Cho and Fryzlewicz (2015)) and the Inspect method (Wang and Samworth (2018)). The following simulations abbreviate the four methods as ECP, KS, SBS, and Inspect. ECP and KS are implemented in the R package: ECP; SBS and Inspect are respectively implemented in the R packages: hdbinseg and InspectChangepoint. We only consider our methods for higher-order tensors due to the lack of competitors. In all simulation experiments, $n = 1800$, $K = 8$ and change point locations are respectively 200, 400, 600, 800, 1000, 1200, 1400, 1600. Each experiment is repeated $N = 200$ times to compute the averages of the estimation \hat{K} , mean squared error (MSE), and the distribution of $\hat{K} - K$. Also, for the accuracy of the estimated locations, we compute the percentage of “correct” estimations in the replications. Following Cho and Fryzlewicz (2015), the estimated change points lie within the distance of $\lfloor \sqrt{n}/2 \rfloor$ from the true change points is considered as the “correct” estimations. We calculate the proportion of all experiments in which at least four true change points were “correctly” estimated, abbreviated as “CP”.

4.1 Order-one tensor

The basic algorithm is described below:

Algorithm 1: Change Point Detection: by using the SF distance of MOSUM

Input: tensor $\mathcal{X} \in \mathbb{R}^{p_1 \times p_2 \times \dots \times p_\kappa}$; $\tau = 0.8$, $\alpha_n = \lfloor \frac{2n^{0.75}}{9} \rfloor$, $\epsilon_n = \frac{(\log n)^{0.55}}{\sqrt{\alpha_n}}$,

$l_n(s) = s(\log n)^{1/2}\epsilon_n$, and $c_n(i) = \frac{s_1\epsilon_n(\log n)^{0.55}}{I(i \in \mathcal{S}) + \frac{1}{n}}$, where $s = 2.5s_1$ and

$s_1 = 1/50$.

- 1 Perform the MOSUM step and then calculate SF distance by (2.3).
- 2 Take the ratio of $\|\mathcal{D}_n(i)\|_s^2 + c_n(i)$ and $\|\mathcal{D}_n(i + \alpha_n)\|_s^2 + c_n(i)$ and obtain $T_n(i)$;
- 3 Identify the intervals using criterion (2.7);
- 4 Filter out the wrong ones by the two conditions in Subsection 2.2.
- 5 Search maximum local minimizers $r_k = \max\{\arg \min_{i \in (m_k(\tau), M_k(\tau))} T_n(i)\}$.

Output: The estimated change points $\{\hat{z}_k = r_k + 2\alpha_n - 1, k = 1, 2, \dots, \hat{K}\}$.

Consider the following model:

$$\mathbf{x}_i = \boldsymbol{\mu}_i + \boldsymbol{\epsilon}_i, \quad (4.1)$$

where $\boldsymbol{\epsilon}_i$ are independent error terms with mean zero, and $p = 50; 100; 500; 1,000; 2,000$.

Data generating mechanism: The data are segmented into nine parts and come from two distributions whose means are $\boldsymbol{\mu}_1$ and $\boldsymbol{\mu}_2$ respectively. $\boldsymbol{\mu}^{(i)} = \boldsymbol{\mu}_1$ for $i = 1, 3, 5, 7, 9$ and $\boldsymbol{\mu}^{(i)} = \boldsymbol{\mu}_2$ for $i = 2, 4, 6, 8$. In the simulations, we consider several scenarios with

- **Dense case:** We consider following cases:

(1) *Strong signals.* $\boldsymbol{\epsilon}_i \sim \mathcal{N}(\mathbf{0}, \mathbf{I}_{p \times p})$. All of the components of vectors $\boldsymbol{\mu}_1$ and

$\boldsymbol{\mu}_2$ are equal to 1.4 and 1 respectively. The magnitude of the signal is then equal to 0.4.

(2) *Weak signals.* $\boldsymbol{\epsilon}_i \sim \mathcal{N}(\mathbf{0}, \mathbf{I}_{p \times p})$. The same setting as above except that all of the components of vectors $\boldsymbol{\mu}_1$ and $\boldsymbol{\mu}_2$ being equal to 1.2 and 1 respectively. The magnitude of the signal is 0.2.

- **Sparse case:** We assume only the first $10\%p$ components of $\boldsymbol{\mu}_1$ and $\boldsymbol{\mu}_2$ are non-zero. $\boldsymbol{\epsilon}_i \sim \mathcal{N}(\mathbf{0}, \tilde{\Sigma})$, where $\tilde{\Sigma} = (\tilde{\sigma}_{ij})$ and $\tilde{\sigma}_{ij} = 0.9^{|i-j|}$. All of the non-zero components of vectors $\boldsymbol{\mu}_1$ and $\boldsymbol{\mu}_2$ are equal to 2 and 1 respectively. The magnitude of the signal is then equal to 1.

- **Mixed distribution case:**

Correlated component case. $\boldsymbol{\epsilon}_i$ in the odd segments follow the standard normal distribution $\mathcal{N}(\mathbf{0}, \tilde{\Sigma})$, and in even segments follow the uniform distribution $U(-1, 1)^p$. All of the components of vectors $\boldsymbol{\mu}_1$ and $\boldsymbol{\mu}_2$ are equal to 2 and 1 respectively.

We have also tried some other settings, such as the cases with dense (or sparse) and strong signals, but elements of the error terms are correlated, and the same settings as sparse and mixed distributions cases except that all elements are independent. As the comparisons with the other methods show similar observations to those from the above simulations, we then report the detailed results in the supplementary materials to save space.

Our method is abbreviated as SFD. The basic information from the simulation results is the following. First, SFD performs better with increasing dimensions, regardless of whether the covariance matrix is identity or non-identity. This dimensionality

bleeding for SFD deserves further study. Second, for all the competitors, the performances are worse when the components of ϵ_i are correlated, and thus, we consider the case with magnitudes being 1. Third, ECP is a strong competitor, particularly when $p \leq 100$ or 500. Fourth, detection in sparse cases is more difficult than in dense instances. Fifth, SFD has, in comparison with the others, similar performance. Therefore, we only report four tables in the main context, and the other three tables are postponed to the Supplementary material.

Table 1. Dense case (signal=0.4; identity covariance matrix): distribution of $\hat{K} - K$.

Scenarios	Procedures	Means	MSE	CP	$\hat{K} - K$						
					≤ -3	-2	-1	0	1	2	≥ 3
(i) $p = 50$	SFD	8.075	0.175	1	0	0	10	165	25	0	0
	ECP	8.080	0.080	1	0	0	0	184	16	0	0
	KS	5.015	10.105	0.395	136	47	14	3	0	0	0
	SBS	9.8	4.73	1	0	2	4	21	51	63	59
	Inspect	8.115	0.175	1	0	0	0	182	14	3	1
(ii) $p = 100$	SFD	8.075	0.075	1	0	0	0	185	15	0	0
	ECP	8.050	0.060	1	0	0	0	191	8	1	0
	KS	4.985	10.155	0.395	144	40	15	1	0	0	0
	SBS	9.985	5.115	1	0	0	2	15	47	71	65
	Inspect	8.09	0.09	1	0	0	0	182	18	0	0
(iii) $p = 500$	SFD	8	0	1	0	0	0	200	0	0	0
	ECP	8.065	0.065	1	0	0	0	187	13	0	0
	KS	4.980	10.250	0.355	140	42	18	0	0	0	0
	SBS	10.265	6.655	1	0	0	0	16	43	52	89
	Inspect	8.060	0.070	1	0	0	0	189	10	1	0
(iv) $p = 1000$	SFD	8	0	1	0	0	0	200	0	0	0
	ECP	8.080	0.080	1	0	0	0	184	16	0	0
	KS	4.960	10.230	0.340	145	42	12	1	0	0	0
	SBS	9.920	5.140	1	0	0	6	14	54	61	65
	Inspect	8.025	0.025	1	0	0	0	195	5	0	0
(v) $p = 2000$	SFD	8	0	1	0	0	0	200	0	0	0
	ECP	8.045	0.045	1	0	0	0	191	9	0	0
	KS	4.985	10.285	0.300	132	55	11	2	0	0	0
	SBS	9.970	5.140	1	0	0	2	17	44	79	58
	Inspect	8.580	1.150	1	0	0	0	122	54	14	10

Table 2. Dense case (signal=0.2; identity covariance matrix): distribution of $\hat{K} - K$.

Scenarios	Procedures	Means	MSE	CP	$\hat{K} - K$						
					≤ -3	-2	-1	0	1	2	≥ 3
(i) $p = 50$	SFD	7.100	1.800	0.925	15	40	60	80	5	0	0
	ECP	8.075	0.105	1	0	0	0	187	12	0	1
	KS	4.835	11.355	0.040	147	38	12	3	0	0	0
	SBS	9.960	5.310	0.985	0	1	4	18	41	71	65
	Inspect	5.515	17.455	0.635	79	24	6	48	34	8	1
(ii) $p = 100$	SFD	7.950	0.400	0.975	0	0	35	150	5	10	0
	ECP	8.08	0.09	1	0	0	0	185	14	1	0
	KS	4.850	10.970	0.020	152	39	8	1	0	0	0
	SBS	9.875	4.845	1	0	0	1	19	61	61	58
	Inspect	7.790	4.880	0.910	20	9	1	105	39	21	5
(iii) $p = 500$	SFD	7.700	0.300	1	0	0	60	140	0	0	0
	ECP	8.050	0.070	1	0	0	0	192	6	2	0
	KS	4.945	10.485	0.070	141	42	17	0	0	0	0
	SBS	10.075	6.005	1	0	0	7	13	47	55	78
	Inspect	8.340	0.970	0.995	1	1	0	141	39	15	3
(iv) $p = 1000$	SFD	7.550	0.600	1	0	15	60	125	0	0	0
	ECP	8.040	0.040	1	0	0	0	192	8	0	0
	KS	4.935	10.565	0.060	139	46	15	0	0	0	0
	SBS	10.040	5.760	1	0	0	2	27	34	62	75
	Inspect	8.220	0.800	0.995	1	0	0	166	17	13	3
(v) $p = 2000$	SFD	7.875	0.125	1	0	0	25	175	0	0	0
	ECP	8.065	0.075	1	0	0	0	188	11	1	0
	KS	4.760	11.590	0.035	158	29	13	0	0	0	0
	SBS	10.140	5.740	1	0	0	0	13	41	72	74
	Inspect	9.020	3.210	1	0	0	0	99	51	24	26

Table 3. Sparse 10%(signal=1; non-identity covariance matrix): distribution of $\hat{K} - K$.

Scenarios	Procedures	Means	MSE	CP	$\hat{K} - K$						
					≤ -3	-2	-1	0	1	2	≥ 3
(i) $p = 50$	SFD	8.045	0.255	1	0	0	19	155	24	2	0
	ECP	8.075	0.145	1	0	1	0	186	9	4	0
	KS	6.515	3.205	1	28	64	77	31	0	0	0
	SBS	9.225	8.135	0.310	7	22	24	34	33	27	53
	Inspect	31.465	641.555	1	0	0	0	0	0	0	200
(ii) $p = 100$	SFD	7.985	0.405	1	0	3	31	134	30	2	0
	ECP	8.040	0.040	1	0	0	0	192	8	0	0
	KS	6.470	3.230	0.995	32	61	84	23	0	0	0
	SBS	9.280	7.030	0.385	3	11	31	43	29	36	47
	Inspect	31.075	621.835	1	0	0	0	0	0	0	200
(iii) $p = 500$	SFD	7.865	0.415	1	0	4	41	135	18	2	0
	ECP	8.070	0.090	1	0	0	0	188	10	2	0
	KS	6.530	2.770	1	19	73	91	17	0	0	0
	SBS	9.535	4.075	0.790	0	0	11	31	57	58	43
	Inspect	19.875	179.565	1	0	0	0	0	0	5	195
(iv) $p = 1000$	SFD	7.980	0.160	1	0	1	15	171	13	0	0
	ECP	8.060	0.060	1	0	0	0	188	12	0	0
	KS	6.475	3.215	0.995	29	67	79	25	0	0	0
	SBS	9.615	4.015	0.940	0	1	8	25	52	69	45
	Inspect	19.200	171.480	1	0	0	0	3	4	6	187
(v) $p = 2000$	SFD	7.995	0.015	1	0	0	2	197	1	0	0
	ECP	8.060	0.070	1	0	0	0	189	10	1	0
	KS	6.495	3.125	1	28	66	81	25	0	0	0
	SBS	9.670	4.320	0.990	1	2	5	23	52	67	50
	Inspect	25.545	407.855	1	0	0	0	0	1	0	199

Table 4. Mixed distribution(non-identity matrix): distribution of $\hat{K} - K$.

Scenarios	Procedures	Means	MSE	CP	$\hat{K} - K$						
					≤ -3	-2	-1	0	1	2	≥ 3
(i) $p = 50$	SFD	8.055	0.135	1	0	0	8	173	19	0	0
	ECP	8.050	0.050	1	0	0	0	190	10	0	0
	KS	7.280	0.950	1	1	20	101	78	0	0	0
	SBS	9.665	4.335	1	0	2	7	31	31	86	43
	Inspect	134.315	17,105.380	1	0	0	0	0	0	0	200
(ii) $p = 100$	SFD	8.040	0.070	1	0	0	3	186	11	0	0
	ECP	8.060	0.060	1	0	0	0	188	12	0	0
	KS	7.385	0.835	1	1	19	82	98	0	0	0
	SBS	9.725	4.505	1	0	0	6	29	48	62	55
	Inspect	234.095	53,133.040	1	0	0	0	0	0	0	200
(iii) $p = 500$	SFD	8	0	1	0	0	0	200	0	0	0
	ECP	8.070	0.080	1	0	0	0	187	12	1	0
	KS	7.360	0.920	1	3	19	81	97	0	0	0
	SBS	9.860	4.930	1	0	1	6	18	50	58	67
	Inspect	610.720	363,921.700	1	0	0	0	0	0	0	200
(iv) $p = 1000$	SFD	8	0	1	0	0	0	200	0	0	0
	ECP	8.050	0.050	1	0	0	0	190	10	0	0
	KS	7.360	0.970	1	3	21	76	100	0	0	0
	SBS	9.920	5.080	1	0	0	3	19	52	61	65
	Inspect	651.650	414,326.100	1	0	0	0	0	0	0	200
(v) $p = 2000$	SFD	8	0	1	0	0	0	200	0	0	0
	ECP	8.040	0.040	1	0	0	0	192	8	0	0
	KS	7.395	0.825	1	2	16	83	99	0	0	0
	SBS	10.120	5.890	1	0	0	1	10	55	65	69
	Inspect	641.365	401,188.600	1	0	0	0	0	0	0	200

4.2 Higher order tensor

We first give the algorithm.

Algorithm 2: Change Point Detection: by using the mode-based SF Frobenius distance of MOSUM

Input: tensor $\mathcal{X} \in \mathbb{R}^{p_1 \times p_2 \times \dots \times p_\kappa}$; $\tau = 0.6$, $\alpha_n = \lfloor \frac{2n^{3/4}}{9} \rfloor$, $\epsilon_n = \frac{(\log n)^{0.55}}{\sqrt{\alpha_n}}$,

$$l_n = s(\log n)^{1/2}\epsilon_n, c_{nl}(i) = \frac{s_1\epsilon_n n^{0.55}}{I(i \in \mathcal{S}_l) + \frac{1}{n}}, s = 10s_1, \text{ and } s_1 = 1/50.$$

- 1 Fix the last mode of \mathcal{X} and then perform the MOSUM step on each mode and then calculate SF distance using the formula in (2.3).
- 2 Take the ratio of $\|\mathcal{D}_{nl}(i)\|_s^2 + c_{nl}(i)$ and $\|\mathcal{D}_{nl}(i + \alpha_n)\|_s^2 + c_{nl}(i)$ and obtain $T_{nl}(i)$;
- 3 Minimize $T_{nl}(i)$ over $1 \leq l \leq p_\kappa$ and then obtain the final statistic $T_n^v(i)$;
- 4 Identify the intervals using the criterion in (2.8);
- 5 Filter out the wrong ones by the conditions in Subsection 2.3.
- 6 Search maximum local minimizers $r_k = \max\{\arg \min_{i \in (m_k^v(\tau), M_k^v(\tau))} T_n^v(i)\}$.

Output: Obtain estimated change points $\{\hat{z}_k = r_k + 2\alpha_n, k = 1, 2, \dots, \hat{K}\}$.

As the literature lacks change point detection methods for general order-two and -three tensors, we only report the simulation results of the two proposed criteria in this paper. Consider the tensor model as

$$\mathbf{X}_i = \boldsymbol{\Sigma}_i + \mathbf{E}_i, i = 1, 2, \dots, n. \quad (4.2)$$

When \mathbf{E}_i is a random matrix whose elements $E_{i,jk}$ are with means zero, the model is order-two. Consider $p_2 = kp_1$ for $k = 1, 16$. Similar observations are made on the simulations with order-three tensors, which are then put in the Supplementary

Materials.

Data generating mechanism: The data are segmented into nine parts coming from two distributions whose means are Σ_1 and Σ_2 respectively. $\Sigma^{(i)} = \Sigma_1$ for $i = 1, 3, 5, 7, 9$ and $\Sigma^{(i)} = \Sigma_2$ for $i = 2, 4, 6, 8$.

In the simulations, each row of \mathbf{E}_i follows $\mathcal{N}(0, \tilde{\Sigma})$ and rows are independent of each other. When $p_2 = p_1$, all elements in Σ_1 and Σ_2 are equal to 1.4 and 1, respectively. Here $p_1 = 10, 30, 50$. The magnitude of the signal is 0.4. When $p_2 = 16p_1$, For $\Sigma_1 = (\sigma_{ij})$, $\sigma_{ij} = 0.8^{|i-j|}$ if $j \leq i$; otherwise, $\sigma_{ij} = 1$. All elements in Σ_2 are equal to 1. Here $p_1 = 10, 12$. For space-saving, the cases with all independent elements and order-three tensors are showed in the Supplementary Materials.

Table 5. Order-two tensor(row correlation): The distribution of $\hat{K} - K$.

Scenario	Procedure	Mean	MSE	CP	$\hat{K} - K$						
					≤ -3	-2	-1	0	1	2	≥ 3
Symmetric cases: $p_1 = p_2$											
$p_1 = 10$	MSFD	3.205	24.805	0.230	188	9	3	0	0	0	0
	SFD	8	0.430	1	0	3	32	129	34	2	0
$p_1 = 30$	MSFD	8.020	0.380	1	0	3	26	136	34	1	0
	SFD	8.005	0.005	1	0	0	0	199	1	0	0
$p_1 = 50$	MSFD	8.295	0.515	1	0	0	7	140	42	9	2
	SFD	8	0	1	0	0	0	200	0	0	0
Asymmetric cases: $p_2 = 16p_1$											
$p_1 = 10$	MSFD	7.365	1.825	0.765	10	34	67	57	25	6	1
	SFD	5.595	7.485	0.920	81	69	41	9	0	0	0
$p_1 = 12$	MSFD	7.960	0.900	0.925	0	14	39	100	36	10	1
	SFD	7.010	1.930	0.995	15	33	82	70	0	0	0

The results reported in Table 5 suggest that the symmetric case favors the SFD-based criterion, whereas the asymmetric case with a much large mode favors the mode-based SFD method. This is also the case when the elements of error matrices are independent. See the Supplementary Material.

5. Application

This section gives two real data examples concerned with order-one and order-two tensors.

5.1 Micro-array Data

We apply our method to a publicly available microarray(aCGH) data set, which has been analyzed in Stransky et al. (2006) and Bleakley and Vert (2011). This data set includes 57 bladder tumor samples. The R package, ECP, provides 43 bladder tumor samples after removing the series that had more than 7% of missing values. The data used for analysis is an $n \times p$ matrix, where $n = 2215$ and $p = 43$. This analysis aims to find important genes. We identify 8 change points at the locations 526, 640, 753, 942, 1158, 1531, 1774, 2054.

5.2 Enron email dynamic network

The CALO project contains data from about 150 users and their email exchanges. The processed data were used in Priebe et al. (2005), based on 184 unique addresses over 189 weeks from 1998 to 2002. The data are available in <https://www.cis.jhu.edu/~parky/Enron/>. We extract the information about the time for sending and receiving

emails from each address during the 189 weeks. We aim to check whether the mail exchange patterns change during this period, reflecting changes in the relationship among these addresses. Each address is regarded as one subject, called the node in networks. The dynamic networks' adjacency matrix $\mathbf{A}_i, i = 1, 2, \dots, 188$ reflects the links between any two subjects. If there is an email exchange between subjects i and j , the (i, j) element of \mathbf{A}_i is 1; otherwise, it is zero.

As this tensor is order-two with $p_1 = p_2$, we first use the SFD-based statistic to detect change points. Three change points are identified at the locations 39, 94, and 141. Thus, the email exchange patterns may change around the 39-th, 94-th, and 141-th weeks. As the sample size is relatively small compared with the size of the tensor, we also use the MSFD-based statistic that identifies the locations 54, 111, and 149. The results from these two methods are similar.

6 Conclusion

In this paper, we propose two criteria to detect change points of tensor data, a signal-screening Frobenius distance (SFD) and a mode-based signal-screening Frobenius distance (MSFD) of MOSUM so that we can handle dense and sparse scenarios. The criteria are based on ratios of FSD's (MSFD's) with adaptive-to-signal ridge functions to enhance the detection capacity. The methods have several advantages: estimation consistency, robustness against distribution and sparsity structure, computational simplicity, and change visualization. Its limitations are mainly in two aspects. We require that the distance between any two changes cannot be too small. The performances of the criteria are relatively sensitive to the choices of s_1 in the ridge and

s in the threshold in the signal-screening Frobenius distance. These deserve further studies.

References

- Al-Sharoa, E., M. Al-Khassaweneh, and S. Aviyente (2017). A tensor based framework for community detection in dynamic networks. In *2017 IEEE international conference on acoustics, speech and signal processing (ICASSP)*, pp. 2312–2316. IEEE.
- Bi, X., X. Tang, Y. Yuan, Y. Zhang, and A. Qu (2021). Tensors in statistics. *Annual review of statistics and its application*, 345–368.
- Bleakley, K. and J.-P. Vert (2011). The group fused lasso for multiple change-point detection. *Technical Report HAL-00602121, Bioinformatics Center (CBIO)*.
- Chen, L., W. Wang, and W. B. Wu (2021). Inference of breakpoints in high-dimensional time series. *Journal of the American Statistical Association*, 1–13.
- Cho, H. and P. Fryzlewicz (2015). Multiple-change-point detection for high dimensional time series via sparsified binary segmentation. *Journal of the Royal Statistical Society: Series B (Statistical Methodology)* **77**, 475–507.
- Kolda, T. G. and B. W. Bader (2009). Tensor decompositions and applications. *SIAM review* *51*, 455–500.
- Mahyari, A. G., D. M. Zoltowski, E. M. Bernat, and S. Aviyente (2017). A ten-

- sor decomposition-based approach for detecting dynamic network states from eeg. *IEEE Transactions on Biomedical Engineering* **64**, 225–237.
- Matteson, D. S. and N. A. James (2014). A nonparametric approach for multiple change point analysis of multivariate data. *Journal of the American Statistical Association* **109**, 334–345.
- Priebe, C. E., J. M. Conroy, D. J. Marchette, and Y. Park (2005). Scan statistics on enron graphs. *Computational & Mathematical Organization Theory* **11**, 229–247.
- Stransky, N., C. Vallot, F. Reyat, I. Bernard-Pierrot, S. G. D. De Medina, R. Segraves, Y. De Rycke, P. Elvin, A. Cassidy, C. Spraggon, et al. (2006). Regional copy number-independent deregulation of transcription in cancer. *Nature genetics* **38**, 1386–1396.
- Venetsanopoulos, A. (2013). -fundamentals of multilinear subspace learning. In *Multilinear Subspace Learning*, pp. 78–99. Chapman and Hall/CRC.
- Wang, D., Y. Yu, and A. Rinaldo (2021). Optimal change point detection and localization in sparse dynamic networks. *The Annals of Statistics* **49**, 203–232.
- Wang, T. and R. J. Samworth (2018). High dimensional change point estimation via sparse projection. *Journal of the Royal Statistical Society: Series B (Statistical Methodology)* **80**, 57–83.
- Zhan, T., Y. Sun, Y. Tang, Y. Xu, and Z. Wu (2021). Tensor regression and image fusion-based change detection using hyperspectral and multispectral images. *IEEE Journal of Selected Topics in Applied Earth Observations and Remote Sensing* **14**, 9794–9802.

- Zhang, F., X. Zhou, and M. Sun (2018). Constrained vcg auction with multi-level channel valuations for spatial spectrum reuse in non-symmetric networks. *IEEE Transactions on Communications* 67, 1182–1196.
- Zhang, W., N. A. James, and D. S. Matteson (2017). Pruning and nonparametric multiple change point detection. In *2017 IEEE international conference on data mining workshops (ICDMW)*, pp. 288–295. IEEE.
- Zhao, W., X. Zhu, and L. Zhu (2021). Detecting multiple change points: a pulse criterion. *Statistica Sinica Accepted*.
- Zhao, Z., L. Chen, and L. Lin (2019). Change-point detection in dynamic networks via graphon estimation. *arXiv preprint arXiv:1908.01823*.